11th International Symposium on Turbulence and Shear Flow Phenomena (TSFP11)
Southampton, UK, July 30 to August 2, 2019

INVESTIGATION OF THE EFFECT OF AN ANISOTROPY-RESOLVING SUBGRID-SCALE MODEL ON BUDGETS OF THE REYNOLDS STRESSES

Ken-ichi ABE
Department of Aeronautics and Astronautics
Kyushu University
744, Motooka, Nishi-ku, Fukuoka 819-0395, Japan
abe@aero.kyushu-u.ac.jp

ABSTRACT

In large eddy simulation (LES), the prediction accuracy of the mean velocity is closely related to that of the ensemble-averaged Reynolds (*Re*) shear stress that consists of the resolved grid-scale (GS) and unresolved subgrid-scale (SGS) parts. It is generally understood that an SGS model plays a role of compensating the lack of the GS part that is originally cut off through a filtering process. Besides this basic role, however, it is expected that an SGS model directly influences instantaneous vortex motions through the momentum equations, leading to a change of the distribution of the averaged GS stresses because the instantaneous fluctuation of the SGS stress is closely related to that of the strain rate in the budget of the GS part. In the present study, to discuss this problem in more detail, an anisotropy-resolving SGS model was carefully investigated. We focused mainly on the contribution of the SGS stress to the prediction accuracy of the ensemble-averaged resolved GS stress through its budget.

INTRODUCTION

In LES, a canonical form of the governing equations for incompressible turbulence may be written as

$$\frac{\partial \overline{U}_i}{\partial t} + \frac{\partial \overline{U}_i \overline{U}_j}{\partial x_j} = -\frac{1}{\rho}\frac{\partial \overline{P}}{\partial x_i} + \frac{\partial}{\partial x_j}\left(2\nu S_{ij} - {\tau_{ij}}^a\right)$$

$$\frac{\partial \overline{U}_i}{\partial x_i} = 0, \qquad S_{ij} = \frac{1}{2}\left(\frac{\partial \overline{U}_i}{\partial x_j} + \frac{\partial \overline{U}_j}{\partial x_i}\right) \tag{1}$$

where $\overline{(\ )}$ denotes a filtered value. In Eq. (1), ρ, $\overline{P}$, $\overline{U}_i$, ν and S_{ij} denote the density, filtered static pressure, filtered velocity, kinematic viscosity and the strain-rate tensor, respectively. Note that ${\tau_{ij}}^a$ is defined as $\tau_{ij} - \tau_{kk}\delta_{ij}/3$, where the SGS stress τ_{ij} is originally expressed as follows:

$$\tau_{ij} = \overline{U_i U_j} - \overline{U}_i \overline{U}_j \tag{2}$$

Therefore, $\overline{P}$ in Eq. (1) includes $\rho\tau_{kk}\delta_{ij}/3$ in this study.

In our previous studies (Ohtsuka and Abe, 2013; Abe and Ohtsuka, 2014), we performed investigations of an anisotropy-resolving SGS model, from which we understood how the extra anisotropic term (EAT) in the SGS model works for enhancing near-wall vortex structures. On the other hand, however, it is still unclear how the SGS model affects the prediction accuracy of the mean velocity that is usually the main purpose of CFD simulations. To answer this question, it is valuable to investigate the effect of the EAT on the budgets of the *Re* stresses.

Considering Eq. (1) being ensemble-averaged, we obtain the following equation:

$$\frac{\partial \left\langle \overline{U}_i \right\rangle}{\partial t} + \frac{\partial \left\langle \overline{U}_i \right\rangle \left\langle \overline{U}_j \right\rangle}{\partial x_j} =$$
$$-\frac{1}{\rho}\frac{\partial \left\langle \overline{P} \right\rangle}{\partial x_i} + \frac{\partial}{\partial x_j}\left(2\nu \left\langle S_{ij} \right\rangle - \left\langle {\tau_{ij}}^a \right\rangle - \left\langle u_i'' u_j'' \right\rangle\right) \tag{3}$$

where $\langle\ \rangle$ denotes an ensemble-averaged value and a value with double prime is its fluctuation, i.e., u_i'' being defined as $u_i'' = \overline{U}_i - \langle \overline{U}_i \rangle$. In Eq. (3), $\left\langle u_i'' u_j'' \right\rangle$ is the resolved *Re* stress and $\left\langle {\tau_{ij}}^a \right\rangle$ is the ensemble-averaged value of ${\tau_{ij}}^a$. To discuss the behavior of the resolved GS part in more detail, we investigate the budget of $\left\langle u_i'' u_j'' \right\rangle$.

From Eqs. (1) and (3), we obtain the transport equation of u_i'', and then the transport equation of $\left\langle u_i'' u_j'' \right\rangle$ can be obtained as follows:

$$\frac{\partial \left\langle u_i'' u_j'' \right\rangle}{\partial t} + \left\langle \overline{U}_k \right\rangle \frac{\partial \left\langle u_i'' u_j'' \right\rangle}{\partial x_k} =$$
$$P_{ij} - \varepsilon_{ij} + \phi_{ij} + \xi_{ij} + \frac{\partial}{\partial x_k}\left(D_{ij} + T_{ij} + J_{ij} + \zeta_{ij}\right) \tag{4}$$

where

$$P_{ij} = -\left\langle u_i'' u_k'' \right\rangle \frac{\partial \left\langle \overline{U}_j \right\rangle}{\partial x_k} - \left\langle u_j'' u_k'' \right\rangle \frac{\partial \left\langle \overline{U}_i \right\rangle}{\partial x_k}, \ D_{ij} = \nu \frac{\partial \left\langle u_i'' u_j'' \right\rangle}{\partial x_k}$$

$$\phi_{ij} = \left\langle \frac{p''}{\rho}\left(\frac{\partial u_i''}{\partial x_j} + \frac{\partial u_j''}{\partial x_i}\right) \right\rangle, \ \xi_{ij} = \left\langle {\tau_{ik}''}^a \frac{\partial u_j''}{\partial x_k} + {\tau_{jk}''}^a \frac{\partial u_i''}{\partial x_k} \right\rangle$$

$$\varepsilon_{ij} = 2\nu \left\langle \frac{\partial u_i''}{\partial x_k}\frac{\partial u_j''}{\partial x_k} \right\rangle, \ \zeta_{ij} = -\left(\left\langle {\tau_{ik}''}^a u_j'' \right\rangle + \left\langle {\tau_{jk}''}^a u_i'' \right\rangle\right)$$

$$T_{ij} = -\left\langle u_i'' u_j'' u_k'' \right\rangle, \ J_{ij} = -\left(\left\langle p'' u_i'' \right\rangle \delta_{jk} + \left\langle p'' u_j'' \right\rangle \delta_{ik}\right) \tag{5}$$

In Eq. (5), ${\tau_{ij}''}^a$ is the instantaneous fluctuation of ${\tau_{ij}}^a$ defined as ${\tau_{ij}''}^a = {\tau_{ij}}^a - \left\langle {\tau_{ij}}^a \right\rangle$. Note that most of the terms except for ξ_{ij} and ζ_{ij} on the right-hand side of Eq. (4) have the same definitions as generally known. Therefore, the two terms, i.e., ξ_{ij} and ζ_{ij}, are newly added in the budget of the resolved *Re* stress in LES. Hereinafter, we call ξ_{ij} the "SGS-strain" term, while ζ_{ij} being the "SGS diffusion" term. It is clearly understood that the instantaneous fluctuations u_i'' and ${\tau_{ij}''}^a$ are closely coupled in these two terms (i.e., ξ_{ij} and ζ_{ij}), and thus not only $\left\langle {\tau_{ij}}^a \right\rangle$ in Eq. (3) but also its fluctuation ${\tau_{ij}''}^a$ is very important for the prediction accuracy of the mean velocity through the budget of $\left\langle u_i'' u_j'' \right\rangle$.

Table 1. Computational parameters for the channel-flow case.

Case	Grid type	Grid numbers	Domain(x-z)	Δx	Δy	Δz
C395A	Finest	513×98×513	$6.4\delta \times 3.2\delta$	0.0125	1×10^{-3} –0.05	0.00625
C395B	Fine	257×98×257	$6.4\delta \times 3.2\delta$	0.025	1×10^{-3} –0.05	0.0125
C395C	Medium	129×98×129	$6.4\delta \times 3.2\delta$	0.05	1×10^{-3} –0.05	0.025
C395D	Coarse	65×98×65	$6.4\delta \times 3.2\delta$	0.1	1×10^{-3} –0.05	0.05
C395E	Fine	257×98×257	$6.4\delta \times 3.2\delta$	0.025	1×10^{-3} –0.05	0.0125
C395F	Medium	129×98×129	$6.4\delta \times 3.2\delta$	0.05	1×10^{-3} –0.05	0.025
C395G	Coarse	65×98×65	$6.4\delta \times 3.2\delta$	0.1	1×10^{-3} –0.05	0.05

Case	Model	Re_τ	Δx^+	Δy^+	Δz^+	Δt
C395A	SMM	395	5	0.4–20	2.5	3×10^{-4}
C395B	SMM	395	10	0.4–20	5	3×10^{-4}
C395C	SMM	395	20	0.4–20	10	5×10^{-4}
C395D	SMM	395	40	0.4–20	20	1×10^{-3}
C395E	EVM	395	10	0.4–20	5	3×10^{-4}
C395F	EVM	395	20	0.4–20	10	5×10^{-4}
C395G	EVM	395	40	0.4–20	20	1×10^{-3}

TURBULENCE MODEL

In this study, for more detailed discussion on the effects caused by an SGS model in LES, we focus on an anisotropic SGS model that was originally proposed by Abe (2013). This model is constructed by combining an isotropic linear eddy-viscosity model (EVM) with an EAT. The SGS stress is modeled as follows:

$$\tau_{ij}{}^a = -2\,\nu_{SGS}\,S_{ij} + 2\,k_{SGS}\,b_{ij}^{EAT} = EVM_{ij} + EAT_{ij} \quad (6)$$

where k_{SGS} and ν_{SGS} are the SGS turbulence energy and the SGS eddy viscosity, respectively. The anisotropy tensor b_{ij}^{EAT} in the EAT of Eq. (6) is modeled as

$$b_{ij}^{EAT} = \frac{\tau'_{ij} - \left(-2\nu' S_{ij}\right)}{\tau'_{kk} - \left(-2\nu' S_{kk}\right)} - \frac{1}{3}\delta_{ij}, \quad \nu' = -\frac{\tau'_{ij}{}^{a} S_{ij}}{2S^2}$$

$$\tau'_{ij} = \left(\overline{U}_i - \widehat{\overline{U}}_i\right)\left(\overline{U}_j - \widehat{\overline{U}}_j\right) \quad (7)$$

where $\tau'_{ij}{}^{a} = \tau'_{ij} - \tau'_{kk}\delta_{ij}/3$ and $S^2 = S_{ij}S_{ij}$. In Eq. (7), ν' is an equivalent eddy viscosity evaluated by an EVM-type linear approximation for τ'_{ij}, which is given by the scale-similarity model of Bardina et al. (1980). Note that $\widehat{(\ )}$ denotes a test-filtered value. Detailed descriptions of the present model are given in Abe (2013).

Considering the fact that the EAT in Eq. (7) yields no undesirable extra energy transfer between the GS and SGS components. This anisotropic SGS model is then expected to successfully predict the SGS-stress anisotropy with no serious effect on the computational stability. Taking account of this modeling process, the present SGS model may be regarded as a combination of a linear EVM and a scale-similarity model with an effective modification for stable computation. In this sense, this type of SGS model can be named ”stabilized mixed model” (SMM, hereafter).

Although the basic performance of the SMM was validated by application to several test cases (Abe, 2013; Abe, 2014), there still remain several points to be further investigated. In this study, we investigate the budget of the ensemble-averaged Re shear stress in Eq. (4), where we focus especially on how the SGS-strain term ξ_{12} influences the prediction of the production P_{12} and pressure-strain ϕ_{12} terms that are the main contributors in the budget of $\left\langle u''v''\right\rangle$.

If we consider a statistically steady-state fully-developed plane channel flow and take $i = 1$ and $j = 2$ in Eq. (4), the production, pressure-strain and SGS-strain terms are expressed as follows:

$$P_{12} = -\left\langle v''v''\right\rangle \frac{\partial\left\langle\overline{U}\right\rangle}{\partial y}, \quad \phi_{12} = \left\langle \frac{p''}{\rho}\left(\frac{\partial u''}{\partial y} + \frac{\partial v''}{\partial x}\right)\right\rangle$$

$$\xi_{12} = \left\langle \left(\tau''^{\,a}_{xx}\frac{\partial v''}{\partial x} + \tau''^{\,a}_{xy}\frac{\partial v''}{\partial y} + \tau''^{\,a}_{xz}\frac{\partial v''}{\partial z}\right) + \left(\tau''^{\,a}_{yx}\frac{\partial u''}{\partial x} + \tau''^{\,a}_{yy}\frac{\partial u''}{\partial y} + \tau''^{\,a}_{yz}\frac{\partial u''}{\partial z}\right)\right\rangle \quad (8)$$

Here, we decompose the SGS-strain term ξ_{12} into the isotropic and anisotropic parts as follows:

$$\xi_{12} = \xi_{12}^{EVM} + \xi_{12}^{EAT} \quad (9)$$

where

$$\xi_{12}^{EVM} = \left\langle EVM''_{1k}\frac{\partial v''}{\partial x_k} + EVM''_{2k}\frac{\partial u''}{\partial x_k}\right\rangle \quad (10)$$

$$\xi_{12}^{EAT} = \left\langle EAT''_{1k}\frac{\partial v''}{\partial x_k} + EAT''_{2k}\frac{\partial u''}{\partial x_k}\right\rangle \quad (11)$$

To make clear the role of the EAT in the SMM, we investigate two types of SGS models in this study. One of the models is the original (full) version of the anisotropic SGS model, and the other is its isotropic EVM version consisting of only the first term on the right-hand side of Eq. (6). In this study, the former full version is referred to as “SMM,” while the latter as “EVM.” We apply these two SGS models to a fully-developed plane channel flow. Note that the left-hand side of Eq. (4) becomes zero for the present test case. The computational parameters are summarized in Table 1. The Reynolds number Re_τ ($= u_\tau\delta/\nu$, u_τ: friction velocity, δ: half channel height) was $Re_\tau = 395$ that corresponds to the DNS of Moser et al. (1999). The computational domain was fixed to be $6.4\delta \times 2\delta \times 3.2\delta$ in the streamwise (x), wall-normal (y) and spanwise (z) directions, respectively. We tested four types of grid nodes in this study, among which the finest grid of 513×98×513 was expected to provide highly-resolved results that are almost the same as those of the DNS. Other computational procedures including the boundary conditions and the numerical schemes are the same as those used in Abe (2013).

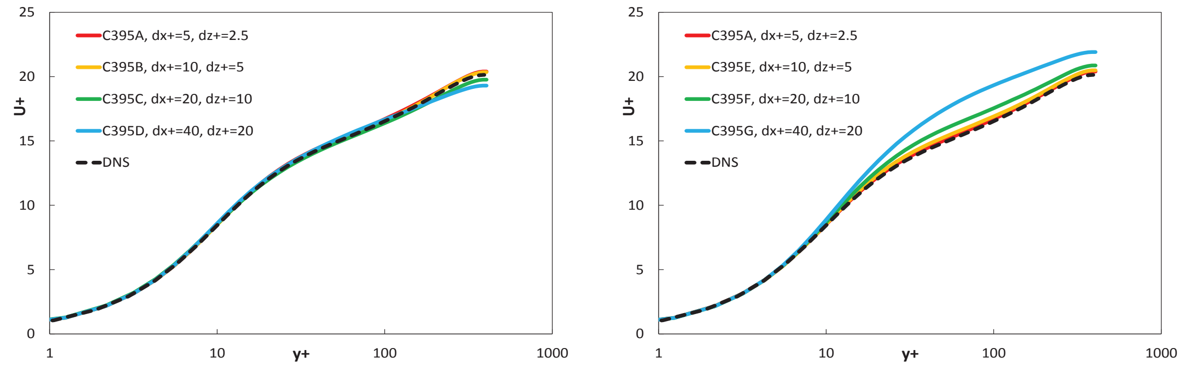

(a) SMM (b) EVM

Figure 1. Comparison of the mean-velocity distributions for various grid resolutions (the finest grid case (C395A) is included in both figures (a) and (b) for reference).

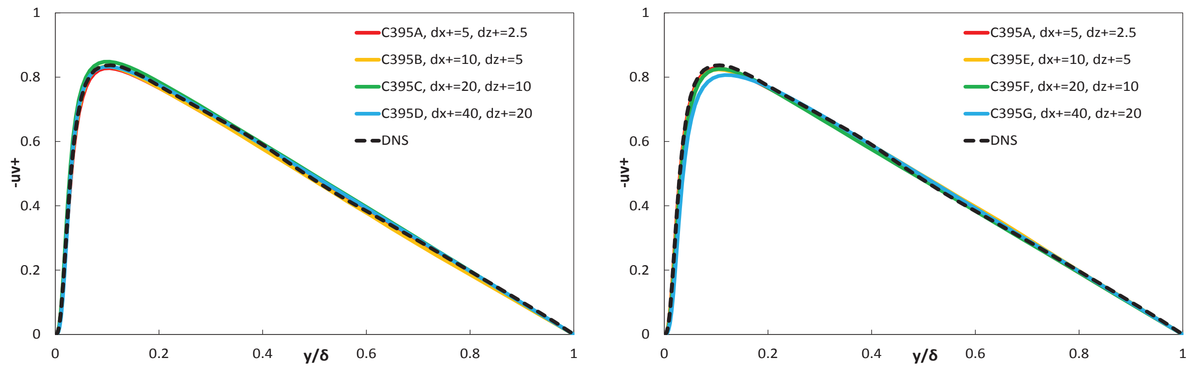

(a) SMM (b) EVM

Figure 2. Comparison of the total (GS+SGS) *Re* shear stress for various grid resolutions.

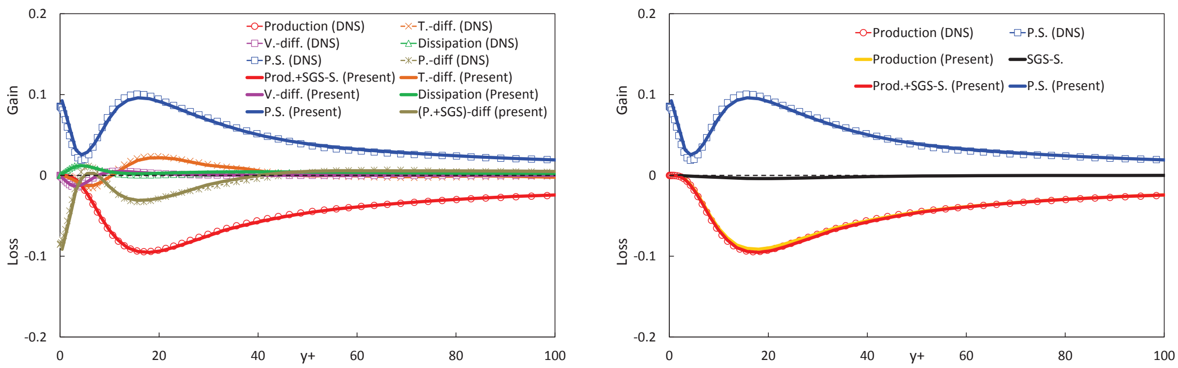

(a) All terms (b) Production and pressure-strain terms

Figure 3. Comparison of the budget of the *Re* shear stress for the finest grid case (C395A) (P.S.: pressure-strain, T.-diff.: turbulent diffusion, P.-diff.: pressure diffusion, V.-diff.: viscous diffusion, SGS-diff.: SGS diffusion, SGS-S.: SGS-strain).

RESULTS AND DISCUSSION

First, to investigate the basic performance of the SGS models tested in this study, Fig. 1 compares the mean-velocity distributions for various grid resolutions. Note that the results for the finest grid-resolution case (C395A) are included in Fig. 1 (b) for reference because the results for C395A are little affected by the SGS model. It is found from Fig. 1 (a) that the results by the SMM correspond well to those of the DNS regardless of the grid resolution. In contrast, as seen in Fig. 1 (b), the performance of the EVM becomes worse as the grid resolution becomes coarser. This kind of decline in the prediction accuracy is rather generally seen in the results of conventional SGS models.

The above feature in the mean-velocity predictions is also confirmed by the comparison of the total (GS+SGS) *Re* shear stress that is shown in Fig. 2. The results predicted by the SMM in Eq. (4) (a) show almost no grid dependency, leading to good prediction of the mean velocity as shown in Fig. 1 (a). On the other hand, however, the results by the EVM in Eq. (4) (b) clearly show underpredictions at around $y/\delta = 0.05$–0.1 (i.e., $y^+ = 20$–40) for coarser grid resolutions.

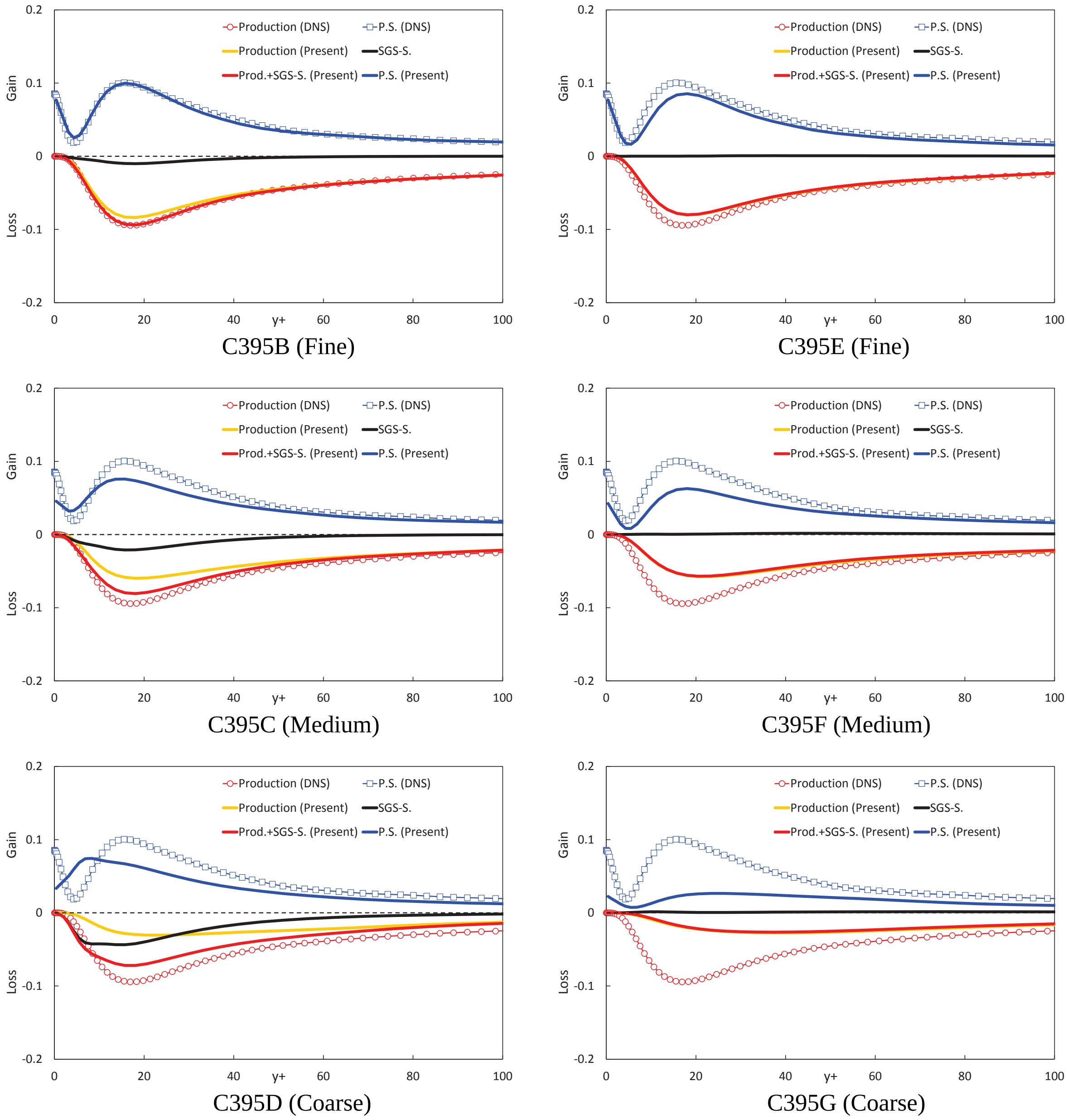

(a) SMM (b) EVM

Figure 4. Contribution of the anisotropic SGS model to the balance between the production and pressure-strain terms in the budget of the *Re* shear stress.

As explained earlier in Eq. (4), the instantaneous fluctuations u_i'' and $\tau_{ij}''^{a}$ are closely coupled in ξ_{ij} and ζ_{ij}. Therefore, we investigate the effect of these correlations on the budget of $\left\langle u_i'' u_j'' \right\rangle$. To validate the basic quality of the present simulation with a sufficient grid resolution, Fig. 3 compares the budget of $\left\langle u'' v'' \right\rangle$ for C395A with that of the DNS data. Figure 3 (a) compares all terms, while Fig. 3 (b) extracts only the production P_{12}, pressure-strain ϕ_{12} and SGS-strain ξ_{12} terms that are the main concerns in this study. As seen in the figure, the present simulation results show fairly good agreement with the DNS data for all terms in the budget. It is also found from Fig. 3 (b) that almost no effect of ξ_{12} is seen in the budget for the finest grid-resolution case.

As mentioned earlier, in what follows, we focus especially on how the SGS-strain term influences the prediction of the production and pressure-strain terms as the grid resolution becomes coarse. Figure 4 compares the results of these terms for various grid resolutions between the SMM and the EVM. As indicated in our previous studies (Ohtsuka and Abe, 2013; Abe and Ohtsuka, 2014), the SGS-stress term must work for enhancing the vortex structures to compensate the lack of the production term in the vorticity-transport equation. Therefore, in the figure, the total amount of the production and SGS-strain terms is also included (i.e., red line) for comparison with the production term of the DNS (red circle). It is found that a definite difference is seen between the SMM and the EVM, particularly in the distributions of the SGS-stress term. Surprisingly, Fig. 4 (b) shows that the SGS-strain term by the EVM gives almost no (or quite small) effect in the budget of $\left\langle u'' v'' \right\rangle$. In contrast, as seen in Fig. 4 (a), the SMM gives a considerable

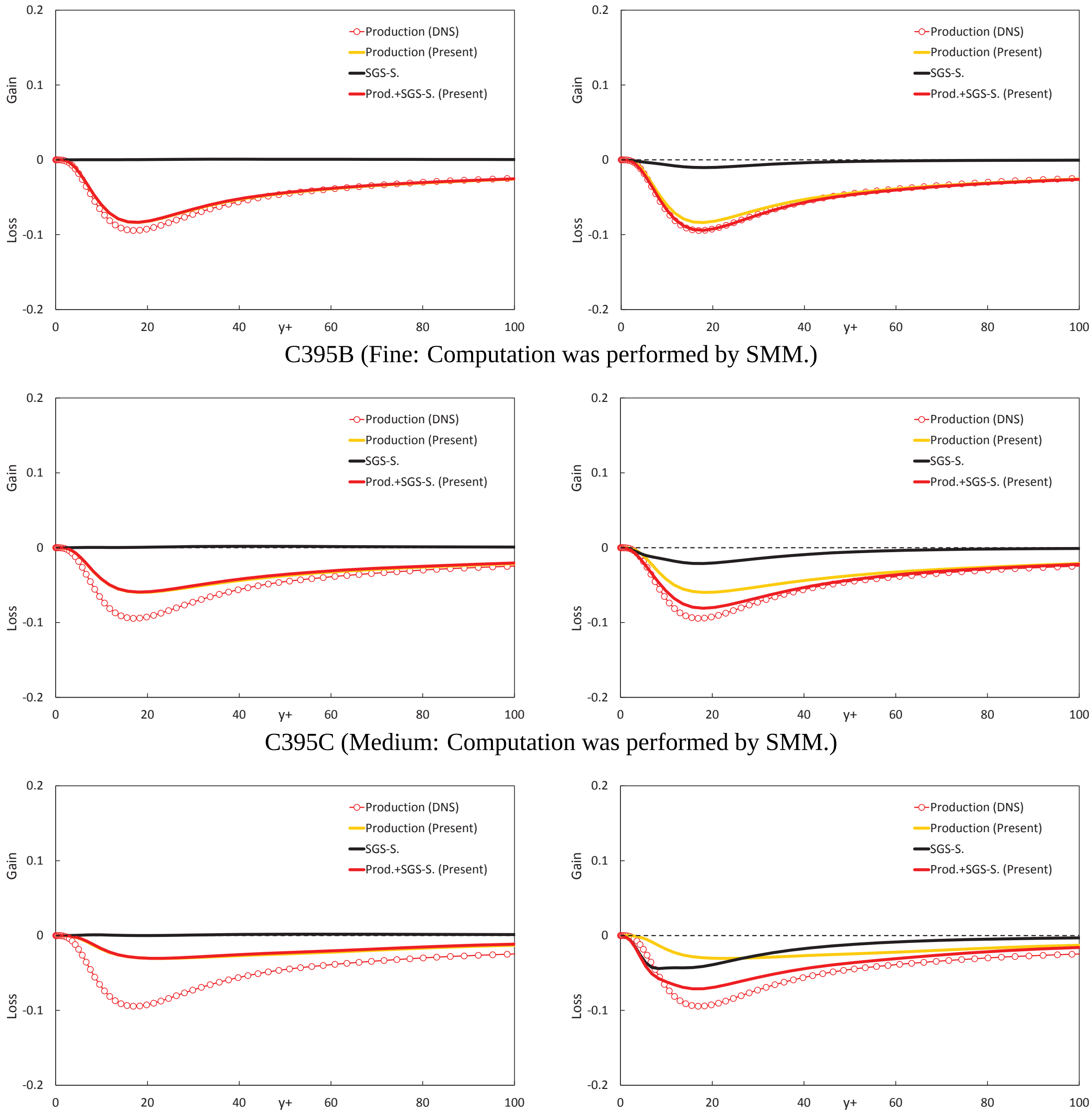

C395B (Fine: Computation was performed by SMM.)

C395C (Medium: Computation was performed by SMM.)

C395D (Coarse: Computation was performed by SMM.)

(a) Isotropic term ξ_{12}^{EVM} in SMM (Eq. (10)) (b) Anisotropic term ξ_{12}^{EAT} in SMM (Eq. (11))

Figure 5. Comparison of the contributions by the isotropic and anisotropic terms in SMM to the SGS-strain term in the budget of the *Re* shear stress. (Black lines: ξ_{ij}^{EVM} on the left-hand side figures, ξ_{ij}^{EAT} on the right-hand side figures, respectively.)

level of the SGS-strain term. Although the distributions of the production term (yellow line) by the SMM look rather similar to those by the EVM, the SGS-strain term compensates the lack of the production term for coarser grid resolutions. This fact corresponds well to the knowledge obtained from our previous studies (Ohtsuka and Abe, 2013; Abe and Ohtsuka, 2014). Consequently, the prediction of the pressure-strain term by the SMM (blue line) is clearly better than that by the EVM, although its accuracy is still far from perfect, particularly in the region close to the wall surface ,i.e., $y^+ < 10$.

As seen in Fig. 4 (a), the SGS-strain term in the SMM is thought to play a role of increasing the production of $\left\langle u''v'' \right\rangle$. Next, to make clearer which of the isotropic part ξ_{12}^{EVM} or the anisotropic part ξ_{12}^{EAT} contributes more largely to generating the SGS-strain term, we decompose the results of ξ_{12} by the SMM into the isotropic and anisotropic contributions, respectively, and compare them in Fig. 5. It is clearly understood from Fig. 5 (a) that even in the results by the SMM, the isotropic part has almost no contribution to generating the SGS-strain term. In contrast, Fig. 5 (b) shows that most SGS-strain term is generated by the effect of the anisotropic part. This is a notable feature of the present anisotropy-resolving SGS model for the improvement of the mean-velocity prediction, in which small grid dependency is achieved compared to conventional isotropic SGS models. Note that another detailed investigation indicates that the largest contribution in ξ_{12}^{EAT} is actually given by the term for $k = 2$ in Eq. (11), that is the anisotropic part of $\left\langle \tau_{xy}''^{\,a} \frac{\partial v''}{\partial y} + \tau_{yy}''^{\,a} \frac{\partial u''}{\partial y} \right\rangle$. Therefore, our next mission for further improvement of the model performance may be to elucidate the relation between this term and instantaneous turbulent flow structures.

As described above, the total amount of the production and SGS-strain terms by the SMM shows much better agreement with the production term of the DNS compared with that by the EVM. In the results by the EVM, ξ_{ij} has almost no value even if the grid resolution becomes coarse, leading to considerable underpredictions for all terms in the budget of $\left\langle u'' v'' \right\rangle$. This may be a reason why the SMM shows relatively small grid dependency compared with isotropic EVM type of SGS models. That being the case, it is strongly expected that anisotropy-resolving SGS models are likely to have the capability of improving the prediction accuracy not only for the modeled part $\langle \tau_{ij} \rangle$ but also for the resolved part $\left\langle u_i'' u_j'' \right\rangle$ thought its budget.

CONCLUDING REMARKS

To elucidate the reason why an anisotropy-resolving SGS model greatly improves the mean-velocity prediction for coarse grid resolutions compared to conventional linear EVM SGS models, we investigated the effect of the anisotropic term on the prediction of the resolved GS stress.

For this purpose, we performed numerical simulations of fully-developed plane channel flows with various grid resolutions at $Re_\tau = 395$. By processing the obtained data, all terms in the budget of the GS *Re* shear stress were calculated. Among them, we focused mainly on a term closely related to the instantaneous fluctuation of the SGS stress, as well as the production and pressure-strain terms that are the primary ones for the gain and loss parts in the budget of $\left\langle u'' v'' \right\rangle$. We compared these results between an anisotropy-resolving SGS model and its linear EVM version.

So far, we have paid attention mainly to the distribution of the ensemble-averaged SGS shear stress $\langle \tau_{12} \rangle$ that directly appears in the transport equation of the mean velocity $\langle \overline{U} \rangle$. From the present study, however, we have found that the fluctuation of the SGS stress coupled with that of the GS strain rate greatly affects the distribution of the resolved GS *Re* shear stress $\left\langle u'' v'' \right\rangle$ through ξ_{12} in Eq. (4).

Since the distribution of $\left\langle u'' v'' \right\rangle$ is most important for the mean-velocity prediction in a wall-shear flow, we carefully investigated the effect of ξ_{12}. We decomposed ξ_{12} into the isotropic and anisotropic parts and their comparison showed that the largest contribution was given by the anisotropic part, while the isotropic part provided almost no value for ξ_{12}. As an isotropic SGS model also showed little effect on the budget of $\left\langle u'' v'' \right\rangle$, this fact may indicate that isotropic EVM type of SGS models essentially have no capability for improving the distribution of the GS *Re* shear stress.

Considering the knowledge obtained from the present study, to improve the prediction accuracy of LES for a wide range of grid resolution, further detailed investigations are thought to be necessary for the effect of an anisotropic part of an SGS model on the budget of the resolved GS stresses.

ACKNOWLEDGMENTS

The present computation was primarily carried out using the computer facilities at the Research Institute for Information Technology, Kyushu University, Japan. This research was supported by a collaborative research program with the research association of Automotive Internal Combustion Engines (AICE) for fiscal year 2019, JSPS KAKENHI Grant Number JP16K05042, JP19K12005 and the “Advanced Computational Scientific Program” of the Research Institute for Information Technology, Kyushu University, Japan.

REFERENCES

Abe, K. (2013), An improved anisotropy-resolving subgrid-scale model with the aid of a scale-similarity modeling concept, *Int. J. Heat Fluid Flow*, Vol. 39, pp. 42-52.

Abe, K. (2014), An investigation of SGS-stress anisotropy modeling in complex turbulent flow fields, *Flow, Turbulence and Combustion*, Vol. 92, pp. 503-525.

Abe, K. and Ohtsuka, T. (2014), On the effect of an anisotropy-resolving subgrid-scale model on turbulent vortex motions, *Proceedings of the 10th International Symposium on Engineering Turbulence Modelling and Measurements*, Marbella, Spain, Paper No. S4-1.

Bardina, J., Ferziger, J.H. and Reynolds, W.C. (1980), Improved subgrid scale models for large eddy simulation, *AIAA Paper*, 80-1357.

Moser , R.D., Kim, J. and Mansour, N. N. (1999), Direct numerical simulation of turbulent channel flow up to Re_τ=590, *Phys. Fluids*, Vol. 11, pp. 943-945.

Ohtsuka, T. and Abe, K. (2013), On the role of an anisotropy-resolving extra term for a subgrid-scale model in near-wall turbulence, *J. Computational Science and Technology*, Vol. 7, pp. 410-425.